


Article

Dispersion Management and Pulse Characterization of Graphene-Based Soliton Mode-Locked Fiber Lasers

Ahmad Fauzi Abas ^{1,*}, Kuen Y. Lau ², Wazie M. Abdulkawi ¹ , Mohammed T. Alresheedi ¹, Farah D. Muhammad ³ and Mohd Adzir Mahdi ⁴

¹ Department of Electrical Engineering, College of Engineering, King Saud University, P.O. Box 800, Riyadh 11421, Saudi Arabia; walkadri@ksu.edu.sa (W.M.A.); malresheedi@ksu.edu.sa (M.T.A.)

² State Key Laboratory of Modern Optical Instrumentation, College of Optical Science and Engineering, Zhejiang University, Hangzhou 310027, China; 0621072@zju.edu.cn

³ Department of Physics, Faculty of Science, Universiti Putra Malaysia, Serdang 43400, Selangor, Malaysia; farahdiana@upm.edu.my

⁴ Wireless and Photonics Networks Research Centre, Faculty of Engineering, Universiti Putra Malaysia, Serdang 43400, Selangor, Malaysia; mam@upm.edu.my

* Correspondence: aabas@ksu.edu.sa

Abstract: This paper presents the generation and characterization of femtosecond pulses utilizing graphene-polymethyl-methacrylate (PMMA) thin-film saturable absorber (SA), which is subjected to different lengths of single-mode fiber (SMF) in an erbium-doped fiber laser cavity. The graphene/PMMA-SA is prepared by using a simple transfer procedure of the thin-film on a fiber ferrule. By increasing the SMF length from 0 to 4 m, the corresponding group velocity dispersion of the entire cavity is estimated to change from -0.033 to -0.121 ps². Analysis of the pulse performance shows that the pulse width behavior varies from 820 fs to 710 fs against different cavity lengths. Similarly, the pulse repetition rate and the spectral bandwidth can be adjusted from 12.5 to 10.0 MHz, and from 8.2 to 5.6 nm, respectively. A comprehensive discussion on the pulse performance is presented, which can contribute to widening the knowledge on the operation of graphene-based soliton mode-locked erbium-doped fiber lasers based on dispersion management by controlling the cavity length.

Keywords: graphene; dispersion management; mode-locking; fiber laser



Citation: Abas, A.F.; Lau, K.Y.; Abdulkawi, W.M.; Alresheedi, M.T.; Muhammad, F.D.; Mahdi, M.A. Dispersion Management and Pulse Characterization of Graphene-Based Soliton Mode-Locked Fiber Lasers. *Appl. Sci.* **2022**, *12*, 3288. <https://doi.org/10.3390/app12073288>

Academic Editors: (John) Xiupu Zhang and Saulius Juodkazis

Received: 4 January 2022

Accepted: 20 March 2022

Published: 24 March 2022

Publisher's Note: MDPI stays neutral with regard to jurisdictional claims in published maps and institutional affiliations.



Copyright: © 2022 by the authors. Licensee MDPI, Basel, Switzerland. This article is an open access article distributed under the terms and conditions of the Creative Commons Attribution (CC BY) license (<https://creativecommons.org/licenses/by/4.0/>).

1. Introduction

Research on ultrafast fiber lasers has been extensively conducted in efforts to reach the optimized design and performance at the highest possible level, which can open up wider possibilities of their applications [1–3]. Among the mechanisms used to generate ultrafast fiber lasers, the saturable absorption effect in passive mode-locking has attracted significant attention due to its advantage of low cost, high stability, high robustness, and good beam quality [4–7]. Contrarily, the active mode-locking technique, which utilizes optical modulator and external electrical devices, has limited flexibility in design. The saturable absorption mechanism in passive mode-locking can be further classified into either natural or artificial saturable absorbers (SAs). Artificial SAs, which are enabled by nonlinear effects occurring in optical fibers, can be driven by several approaches, such as nonlinear polarization rotation [8,9], nonlinear amplifying loop mirror [10–12], and nonlinear optical loop-mirror [1]. They can offer automatic self-start-up of mode-locked operation even without manual triggering conditions, as required by most of their natural analogs [1]. Furthermore, their properties of a high damage threshold and easy implementation in a fiber laser cavity are also attractive factors. However, there is still a considerable challenge in achieving the shortest possible pulse duration by using this technique, and their vulnerability towards environmental changes also still remains a problem. Concurrently,

passive mode-locking by natural saturable absorbers has emerged as the preferred strategy to generate ultrashort pulse, due to their excellent optical properties and high compatibility with fiber laser systems.

Recently, various kinds of materials from the group of topological insulators [13–15], transition metal dichalcogenides [16–19], and transition metal oxides [20,21] have been widely explored and demonstrated as new potential saturable absorbers. MXenes, black phosphorus, metal-organic frameworks, bismuthene, and antimonene are among the 2D materials that have attracted considerable research interest in their application as saturable absorbers due to their unique optical properties [22–25]. It is important to point out that the rise and advancement of these materials has been initiated following the success of graphene, the pioneer of all 2D materials as a versatile saturable absorber, which is still remarkable to date [26–29]. The superiority of graphene for saturable absorber applications, which is highlighted in the recent review by X. Peng et al. [30], also deserves to be mentioned. It is undeniable that graphene possesses a short recovery time, zero bandgap energy, ultra-broadband absorption, gapless linear dispersion of Dirac electrons, high modulation depth, and wide absorption wavelength bandwidth, which are desirable for femtosecond pulse generation [30].

In general, femtosecond pulse lasers realized by soliton mode-locking are very useful for absolute distance measurement [31], optical sensing [32], and coherent communication [33] due to their high laser stability and high pulse quality with a low chirp. The net anomalous dispersion from the soliton-based mode-locked regime is an advantage in balancing the mutual effect of dispersion and non-linear Kerr effect imposed on the pulse propagation [34]. In expanding the capability of soliton mode-locked fiber lasers, several attempts have been made to produce tunable pulse width, repetition rate, or spectral bandwidth of the laser output [35,36], which are normally achieved by introducing the filtering effect. However, the dependence of the aforementioned pulse characteristics on cavity dispersion has not been thoroughly determined. Thus, analysis of the spectral and temporal characteristics of the output pulses based on the net cavity dispersion is still necessary. This has led to research progress on tuning the net cavity dispersion for optimizing the output pulse between negative and normal dispersion regime [37], as well as within the stretched-pulse regime [38] in thulium- and holmium-doped fiber lasers, respectively. In this regard, there is still room for knowledge enhancement to further investigate the similar tuning effect in other dynamics of fiber lasers, particularly within the anomalous dispersion regime.

We are interested in investigating the dispersion behavior in graphene-based soliton mode-locked erbium-doped fiber lasers (EDFL), and its influence on the pulse performance by tailoring the cavity length. For this purpose, the length of single-mode fibers (SMF) in the cavity is reduced gradually from 4 m to 0 m while keeping other fiber lengths constant. The mode-locked operation is enabled by graphene/PMMA thin film as SA, which is prepared by using a simple transfer procedure of the thin-film on a fiber ferrule. The laser and pulse characteristics are investigated within the net cavity dispersion ranging from -0.033 to -0.121 ps², which falls in the anomalous dispersion regime. Pulse duration as short as 710 fs is generated from this proposed laser at the net dispersion closest to zero, while the maximum energy of 599.52 pJ is obtained at the highest value of the anomalous dispersion.

2. Structural Characterization of Graphene Polymer Thin Film (GPTF)

In this work, the graphene material is obtained from ACS Material, LLC which takes the form of a bilayer structure, consisting of polymethylmethacrylate (PMMA) as the protective layer to the graphene layer deposited on a polymer substrate. Figure 1a–c shows the purchased Trivial Transfer GrapheneTM, its schematic structure, and 3D profiler image of graphene polymer thin film (GPTF), respectively. As can be seen from Figure 1c, there are two distinctive colored areas: “blackish” and rainbow-like. The “blackish” region indicates the polymer substrate with non-uniform thickness, whereas the interference-induced rainbow-colored region denotes the graphene/PMMA thin film. The thin-film

interference is generated by the path difference of the light ray refraction phenomenon at the air-PMMA boundary close to the polymer substrate.

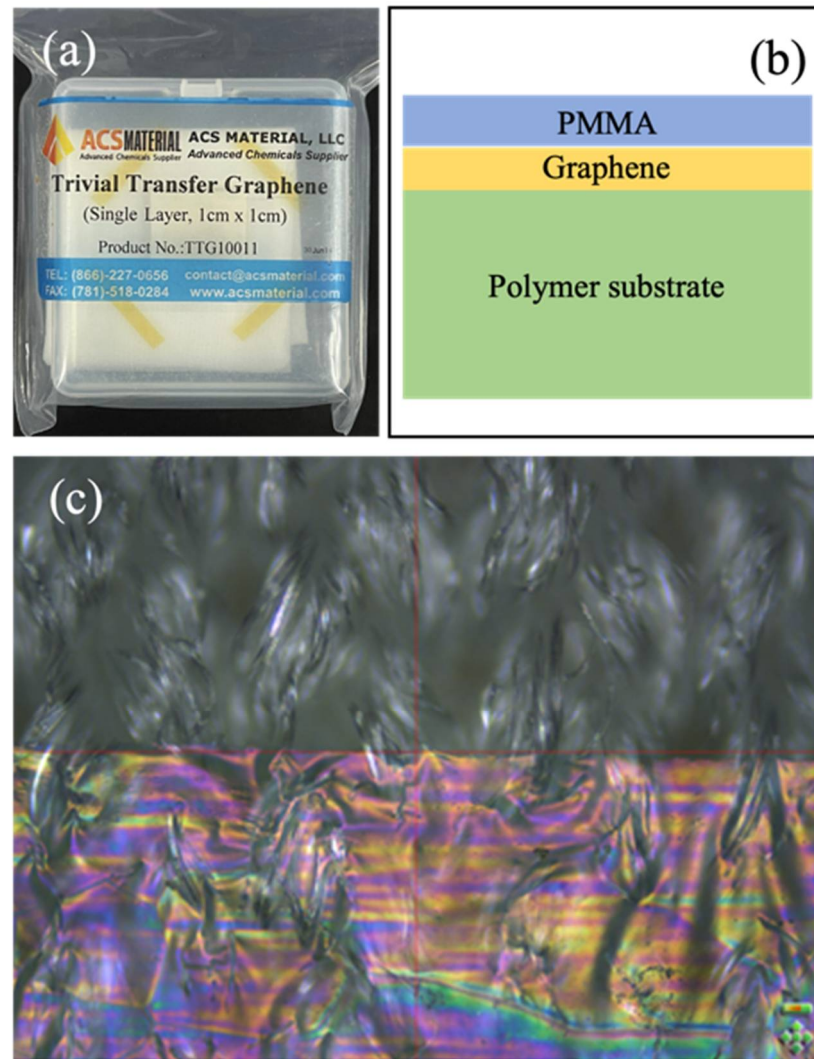


Figure 1. (a) Trivial Transfer GrapheneTM, (b) schematic diagram, and (c) 3D profiler image of GPTF (PMMA and graphene layer) on polymer substrate.

3. Fabrication of Graphene/PMMA-SA

First and foremost, the GPTF is detached from the polymer substrate using drops of deionized (DI) water. This wet GPTF is then placed on a filter paper before cutting it into a size of 1 mm × 1 mm, as shown in Figure 2a, to be placed on a fiber facet. Through the adhesion effect, the GPTF remains stuck to the fiber facet. The wet filter paper is then removed from the GPTF by using tweezers, as shown in Figure 2b, and the GPTF is left to dry on the fiber facet for five minutes, as shown in Figure 2c. Finally, the fiber ferrule with the GPTF is connected to another clean fiber ferrule through a fiber adaptor to form the sandwich-structured graphene/PMMA-SA, as illustrated in Figure 2d.

The composition of the transferred GPTF on the fiber ferrule is characterized by using EDX spectroscopy, and the result is illustrated in Figure 3. The elements “Si” and “O” indicate the bare element of silica optical fiber, with their respective weight percentage of 19.62% and 33.15%. The presence of element “Zr” with a weight percentage of 12.56% originates from the ceramic zirconia fiber ferrule. The element “Ge” is the germanium ions for silica fiber dopant. Graphene material, represented by element “C”, remarks the highest weight percentage of 34.67%. The high purity of each material composition

has been confirmed based on the absence of other chemical elements observed from the EDX spectrum.

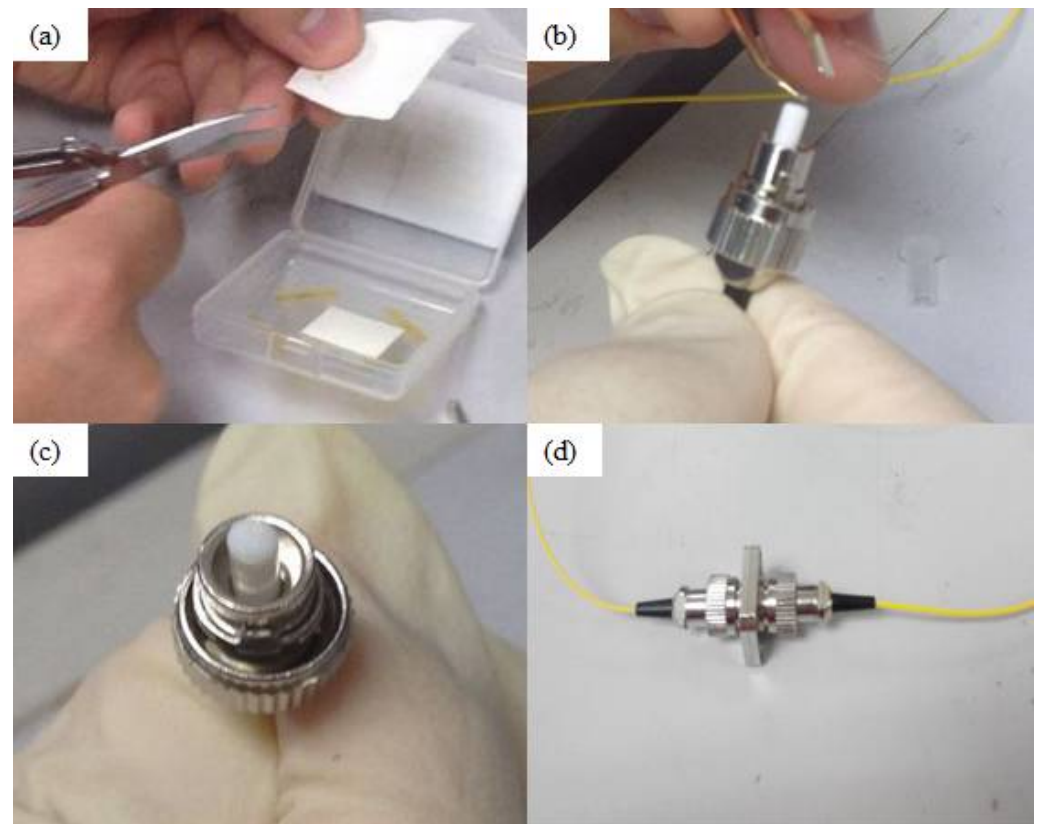


Figure 2. (a–d) Fabrication procedures of graphene/PMMA-SA.

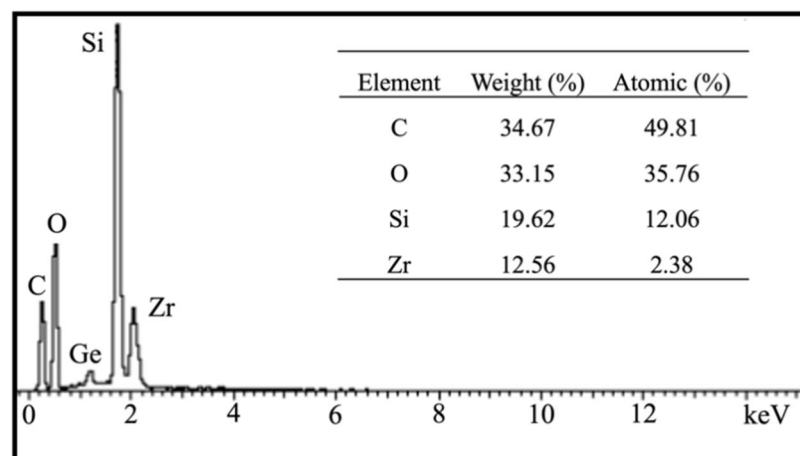


Figure 3. EDX spectra of the deposited GPTF on a fiber core.

4. Optical Characterization of Graphene/PMMA-SA

The optical transmission measurement of the graphene/PMMA-SA is carried out by using a broadband amplified spontaneous emission (ASE) source (Amonics ALS-CL-17-B-SC), and a Yokogawa AQ6370B optical spectrum analyzer (OSA) within a 1525 to 1656 nm wavelength range. Figure 4 shows the result of the measurement, which indicates that the transmission loss of the graphene/PMMA-SA is less than 0.6 dB across the entire wavelength range. Previous reports have proved graphene to be the broadband SA, which could cover as wide as a 1000 nm to 2000 nm wavelength range [39]. However, the charac-

terization of graphene/PMMA-SA beyond the C-band region could not be demonstrated due to the operational wavelength limitation of the available OSA and ASE source used in this work.

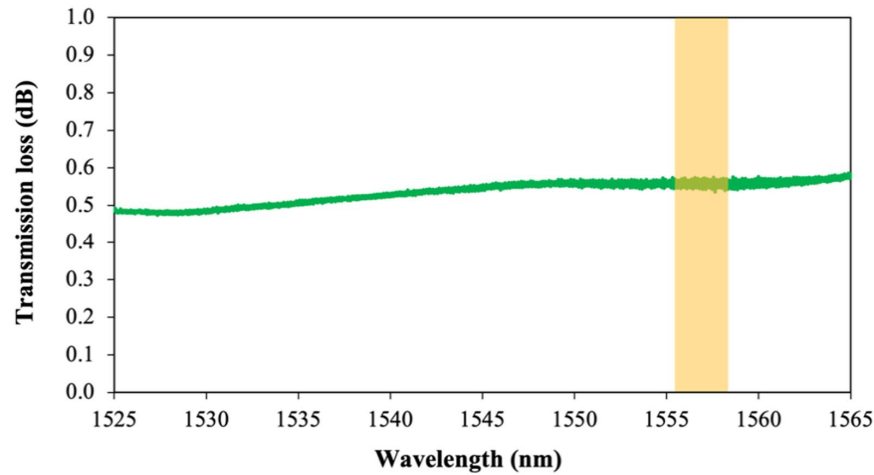


Figure 4. Transmission loss of graphene/PMMA-SA across C-band wavelength region.

The nonlinear optical properties of the graphene/PMMA-SA are characterized by employing a balanced twin detector method, which consists of an M-fiber Menlosystem pulsed fiber laser source with a central wavelength of 1560 nm, pulse repetition rate of 250 MHz, and pulse duration of 117 fs. Figure 5 illustrates the nonlinear saturable absorbance of graphene/PMMA-SA, which can be well-fitted by a solid curve based on the nonlinear saturable absorbance formula [40], as expressed in Equation (1),

$$\alpha(I) = \frac{\alpha_0}{1 + \frac{I}{I_{sat}}} + \alpha_{ns} \tag{1}$$

where $\alpha(I)$ is the intensity-dependent absorption coefficient, I_{sat} is the saturation intensity, α_0 is the saturable absorbance (modulation depth, MD), I is the peak intensity, and α_{ns} is the non-saturable absorbance. Based on the curve fitting, the modulation depth and saturation intensity of graphene/PMMA-SA are estimated to be approximately 0.8% and 2.2 MW/cm², respectively. This encourages great prospects of the graphene/PMMA-SA to perform effectively in generating ultrafast fiber lasers. In addition, the PMMA also holds graphene firmly in place on the fiber facet to ensure its interaction with the waveguided light.

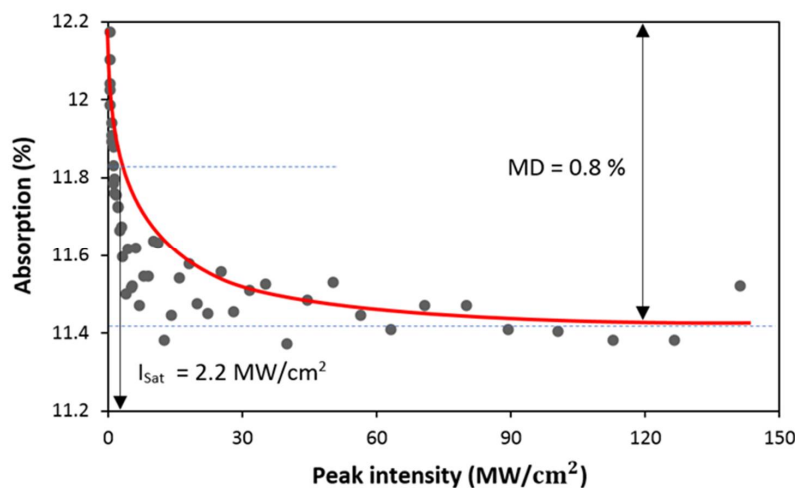


Figure 5. Nonlinear saturable absorbance properties of graphene/PMMA-SA.

5. Experimental Setup

Figure 6 shows the experimental setup of graphene-based mode-locked EDFL. The laser cavity initially consists of 5 m long Lucent HP980 EDF, 1 m long Corning Hi-1060 fiber, and 10.4 m long Corning SMF-28. The EDF, which has a signal absorption coefficient of 3.5 dB/m at 1530 nm, is pumped by a 975 nm laser diode (LD) with a maximum operating power of approximately 100 mW via a 980/1550 nm wavelength division multiplexer (WDM). Two isolators, namely ISO-1 and ISO-2, are used to ensure unidirectional signal oscillation within the cavity in an anti-clockwise direction. The graphene/PMMA-SA fabricated in this work is placed in between ISO-1 and ISO-2. Since the fabricated SA is based on sandwiched-type thin film, there is a possibility of Fresnel reflection at the interface between fiber ferrule and the thin film itself. In this setup, ISO-1 is utilized to prevent the Fresnel reflection from entering the EDF. On the other hand, ISO-2 is employed to ensure that the backward light propagation from the EDF cannot reach the graphene/PMMA-SA, which leads to another Fresnel reflection phenomena. A polarization controller (PC) is used to control the polarization state of the signal, which is connected to the output of ISO-2. A 3-dB coupler is used to tap out 50% of the signal for analysis, while the other 50% of the signal is channeled back to the WDM to form the laser cavity. Analysis of the net cavity dispersion and the output performance commences with the additional SMF length of 4 m in the cavity. The additional SMF is trimmed by 0.5 m for each trial until the length is finally reduced to 0 m. The optical spectrum is measured by the OSA. The pulse train is monitored by a digital phosphor oscilloscope (Tektronix TDS 3012C) through a D-8IR Picometrix photodetector. The radio frequency (RF) signal is monitored by an RF spectrum analyzer (GW INSTEK GSP-830). Measurement of the pulse duration is performed by using an Alnair HAC-200 autocorrelator.

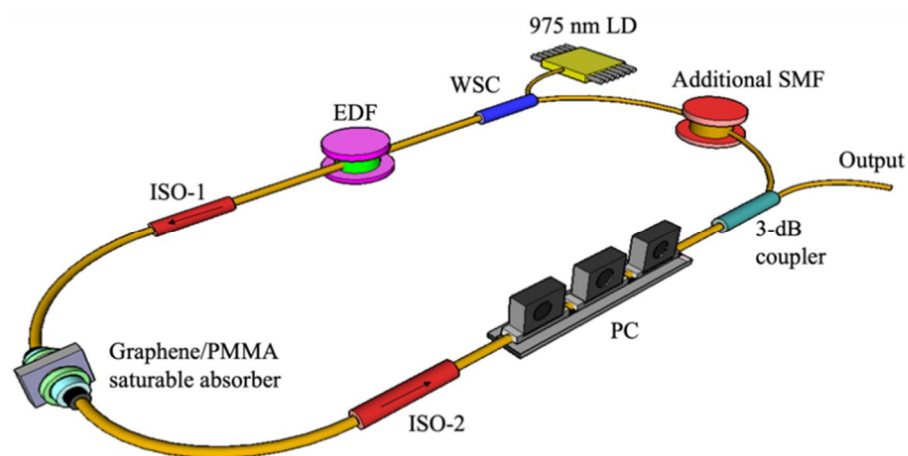


Figure 6. Experimental setup of graphene-based mode-locked EDFL.

6. Dispersion Management of the Mode-Locked Laser

The dispersion coefficient, β_2 of the SMF-28, Hi-1060 fiber and EDF at 1550 nm are $-22 \text{ ps}^2/\text{km}$, $-7 \text{ ps}^2/\text{km}$, and $23 \text{ ps}^2/\text{km}$, respectively. The estimated net group velocity delay (GVD), according to a different total length of SMF-28 that ranges from 10.4 m to 6.4 m in the cavity, is shown in Table 1. Starting from the net GVD value of -0.121 ps^2 for 10.4 m long SMF-28, it can be seen that every decrease of 0.5 m length results in a constant increase in the net GVD of approximately 0.011 ps^2 . This corresponds to a net GVD of -0.033 ps^2 at the shortest SMF-28 length of 6.4 m. It can be deduced that while all the net GVD values obtained lie in the anomalous dispersion regime, the value trends towards zero-dispersion with shorter lengths of the SMF-28. For a real dispersion managed fiber laser, the net cavity dispersion is made to switch from anomalous dispersion to near-zero dispersion, and, subsequently, to net-normal dispersion, as reported in Refs. [10,41]. This results in a large change in pulse operation regime from soliton to stretched-pulse, and to dissipative soliton mode-locking, respectively.

Table 1. Estimated net GVD against different lengths of SMF-28.

Fiber Length (m)			Fiber GVD (ps ²)			Net GVD (ps ²)
SMF-28	EDF	Hi-1060	SMF-28	EDF	Hi-1060	
10.4			−0.23			−0.121
9.9			−0.22			−0.110
9.4			−0.21			−0.099
8.9			−0.2			−0.088
8.4	5	1	−0.19	0.115	−0.007	−0.077
7.9			−0.17			−0.066
7.4			−0.16			−0.055
6.9			−0.15			−0.044
6.4			−0.14			−0.033

7. Results and Discussions

With appropriate PC adjustment, a stable self-starting mode-locked fiber laser is achieved at the pump power of 27.1 mW. Figure 7 shows the mode-locked characteristics of the fiber laser taken for 2 m length of additional SMF-28 at a pump power of 80 mW. As measured from the OSA, the mode-locked output spectrum has a central wavelength of 1556.2 nm, which matches the gain profile of the EDF [42], and a 3-dB bandwidth of 7.47 nm, as shown in Figure 7a. The existence of multiple Kelly's sidebands validates that the pulse belongs to conventional soliton. By using a sech^2 fitting in the autocorrelation trace, the full width at half maximum pulse duration (t_{FWHM}) is 730 fs (Figure 7b). The experimental result agrees well with the theoretical sech^2 curve fitting, with no indication of pulse breaking or pulse pair generation, thus confirming the soliton-like operation of the mode-locked pulse. The corresponding time-bandwidth product (TBP) is estimated to be 0.676. The pulse train measured from the oscilloscope is shown in Figure 7c, where the pulse repetition rate and the time interval between pulses are 11.19 MHz and 0.0894 μs , respectively. The absence of spectral modulation proves that the Q-switching instability does not exist, thus verifying good stability of the mode-locked pulse operation. From the RF measurement, the peak-to-pedestal extinction ratio (PER) at the fundamental repetition rate is approximately 41 dB, which is measured with about 1 MHz frequency span and 30 kHz resolution bandwidth, as shown in Figure 7d. The central frequency of the fundamental pulse is about 11.19 MHz, which is tallied with the value obtained from the oscilloscope trace. The RF spectrum with a span of 200 MHz is shown in Figure 7e, which indicates an evenly spaced frequency interval of approximately 11.19 MHz, thus further verifying the stability of the mode-locked pulse operation.

Similarly, we experimentally investigate the mode-locked output characteristics at other lengths of the SMF-28. The spectral bandwidth of the optical spectrum for every different length of the SMF-28 is measured, and the results are divided into three distinct regions according to a degree of the wideness of the spectral bandwidth, as shown in Figure 8. Each region corresponds to a certain range of spectral bandwidth, with only slight variation between one another. Region 1 has the broadest spectral bandwidth of more than 8 nm, which is achieved when employing the additional SMF-28 length of 0 m and 0.5 m. A narrower spectral bandwidth of approximately 7.5 nm is measured in Region 2, which consists of 1 to 2.5 m of the additional SMF-28. The narrowest spectral bandwidth is acquired between 5.5 and 6 nm when the SMF-28 length is above 3 m, as shown in Region 3. This infers that the spectral bandwidth increases when the SMF-28 length decreases, corresponding to the increment of the net GVD negative value.

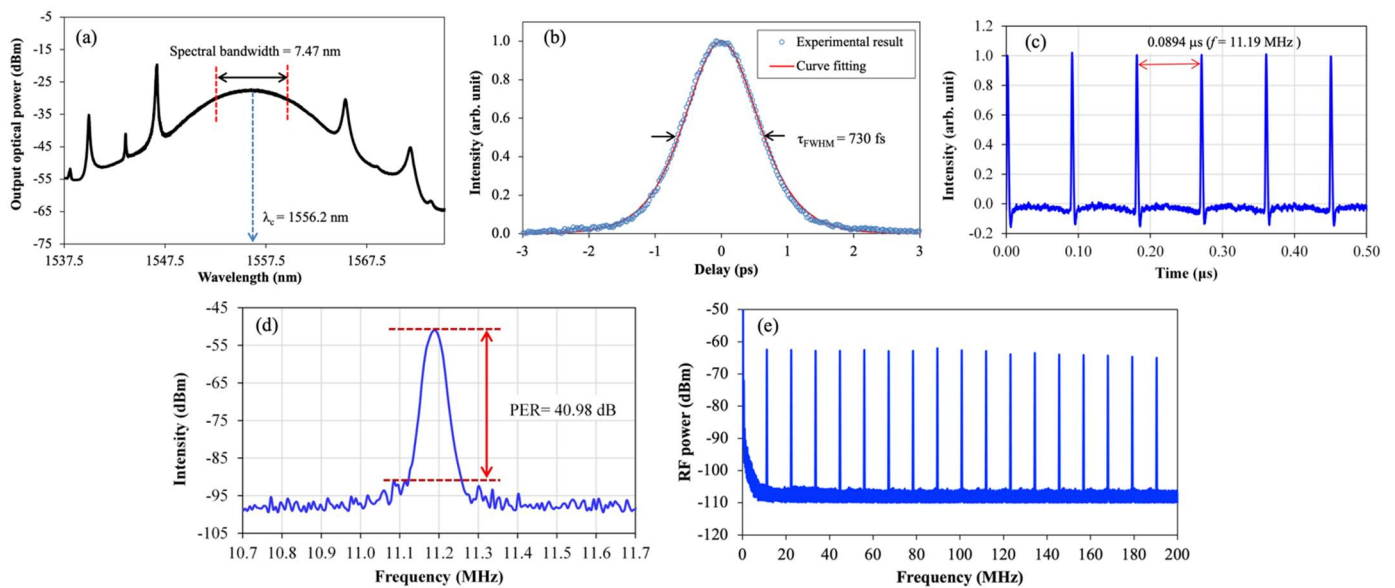


Figure 7. Mode-locked output characteristics; (a) optical spectrum, (b) autocorrelation trace, (c) pulse train, (d) RF spectrum at the fundamental frequency peak, and (e) RF spectrum at 200 MHz span.

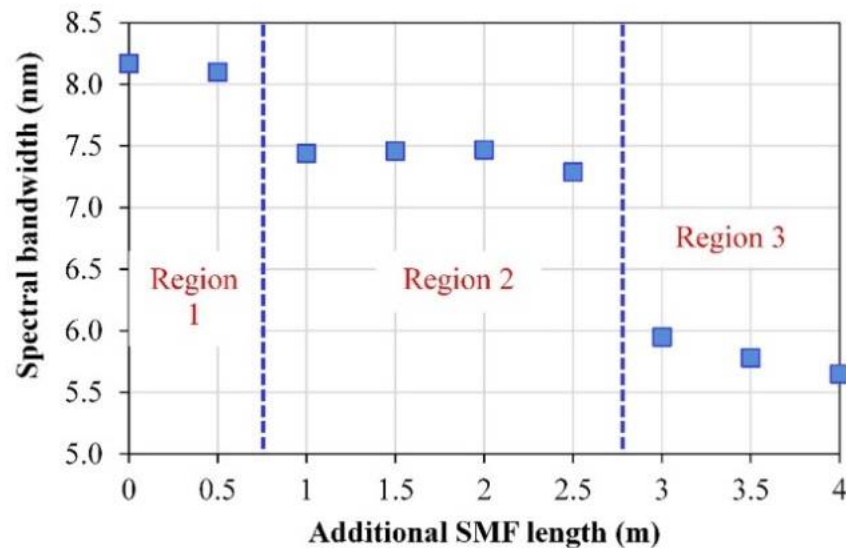


Figure 8. Spectral bandwidth of the laser output against different SMF-28 lengths.

The pulse repetition rate behavior for different SMF-28 lengths taken at the same pump power of 80 mW is plotted in Figure 9. A decreasing pattern of the pulse repetition rate from 12.5 to 10.0 MHz is observed, with a consistent interval of about 0.3 MHz for every increase of 0.5 m length SMF-28. This justifies that the experimental value of the pulse repetition rate matches well with the computed pulse cavity round-trip time for each total cavity length that ranges from 11.4 to 15.4 m.

Analysis of the pulse duration against different lengths of SMF-28 is made based on the graph plotted in Figure 10. The experimental findings show that a shorter pulse duration of the mode-locked EDFL is attained with a shorter cavity length, from the highest value of 820 fs at 4 m length additional SMF-28, to the lowest value of 710 fs at 0 m additional SMF-28. This agrees with the inverse correlation between pulse duration and spectral bandwidth of the mode-locked EDFL, as presented in Figure 8. The corresponding TBP value decreases gradually from 0.719 to 0.573, with increasing SMF-28 length from 0 to 4 m. All the obtained TBP values for all SMF-28 lengths are slightly higher from the expected transform-limited sech^2 pulse of 0.315, which indicates minor chirping in the pulse due to

residual dispersions in the laser cavity. Since the TBP value decreases with SMF-28 length, the minor chirping is deduced to be inversely proportional to the length of SMF-28.

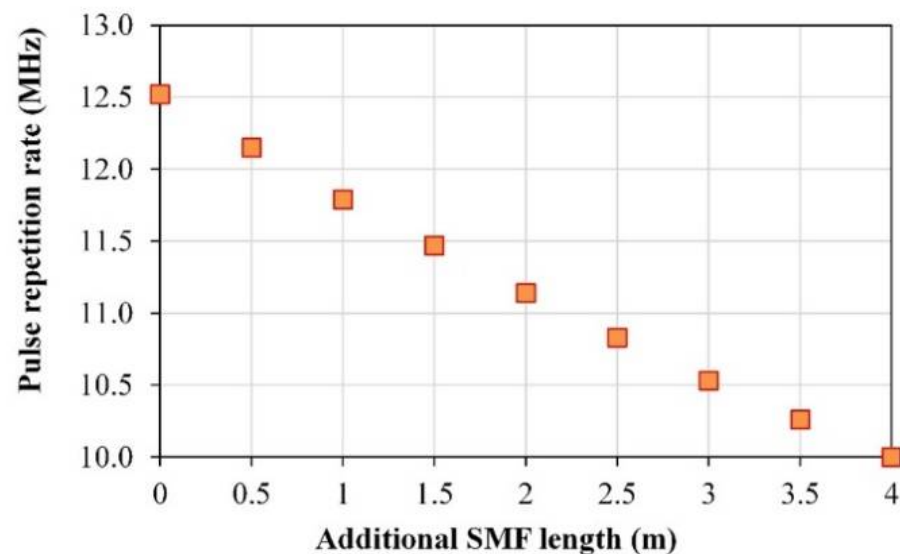


Figure 9. Fundamental pulse repetition rate at various additional SMF-28 lengths.

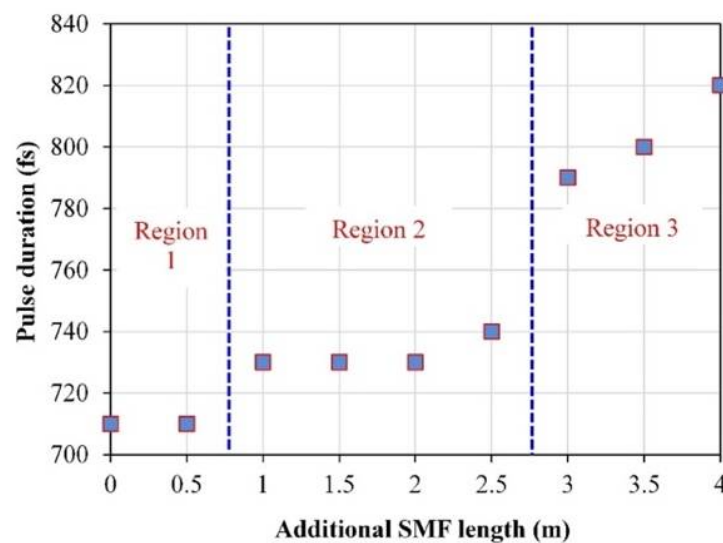


Figure 10. Pulse duration measurement at different additional SMF-28 lengths.

The pulse stability of the mode-locked EDFL at different SMF-28 lengths is examined by analyzing the PER of the RF signal at the first-order pulse. In this measurement, the RF spectrum analyzer is set to a span of 1 MHz and a resolution bandwidth of 30 kHz. Figure 11 shows the recorded PER value based on different lengths of SMF-28 used. It is observed that the PER value fluctuates across 0 to 4 m range of the SMF-28 length, with the maximum value of 40.98 dB obtained at 2 m length, and the minimum value of 39.88 dB recorded at 0.5 m length.

The development of the average output power and pulse energy against pump power for different additional SMF-28 lengths are shown in Figure 12a,b, respectively. From Figure 12a, it can be observed that after reaching the similar continuous wave (CW) lasing threshold of 12.8 mW, all the graphs exhibit a linear increment of the average output power with respect to the pump power. As for the case of pulse energy evolution in Figure 12b, starting from the mode-locking threshold of 27.1 mW, the pulse energy increases linearly with respect to pump power for all different lengths of the SMF-28. The mode-locking

threshold achieved in this work is relatively low for a graphene-based mode-locked fiber laser in the C-band region [43–45], which is attributed to the low transmission loss of the fabricated graphene/PMMA thin film of 0.6 dB. From the perspective of the average output power and pulse energy variation with respect to the length of additional SMF-28, it can be deduced that the longer the fiber, the higher the resulting average output power and pulse energy. Based on the results, the value of maximum average output power, maximum pulse energy, and power slope efficiencies for each respective length of additional SMF-28 are tabulated in Table 2. The maximum average output power and maximum pulse energy increases from 4.93 to 5.99 mW and from 391.47 to 599.52 pJ, respectively, as the SMF-28 length increases from 0 to 4 m. It must be noted that the maximum average output power and pulse energy are not limited to these values, and higher values are expected to be obtained if a laser diode with a higher pump power is used. However, since this work is limited by a maximum available pump power of ~100 mW, further demonstration of the average output power and pulse energy above that pump power could not be demonstrated. Similarly, the power slope efficiency also increases from 5.70% to 6.76% with the increase in SMF-28 length.

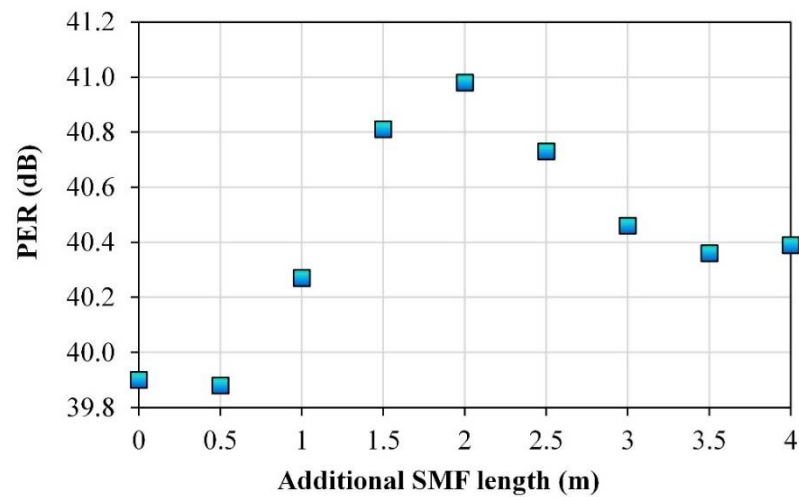


Figure 11. PER measurement of the mode-locked signal at different additional SMF-28 lengths.

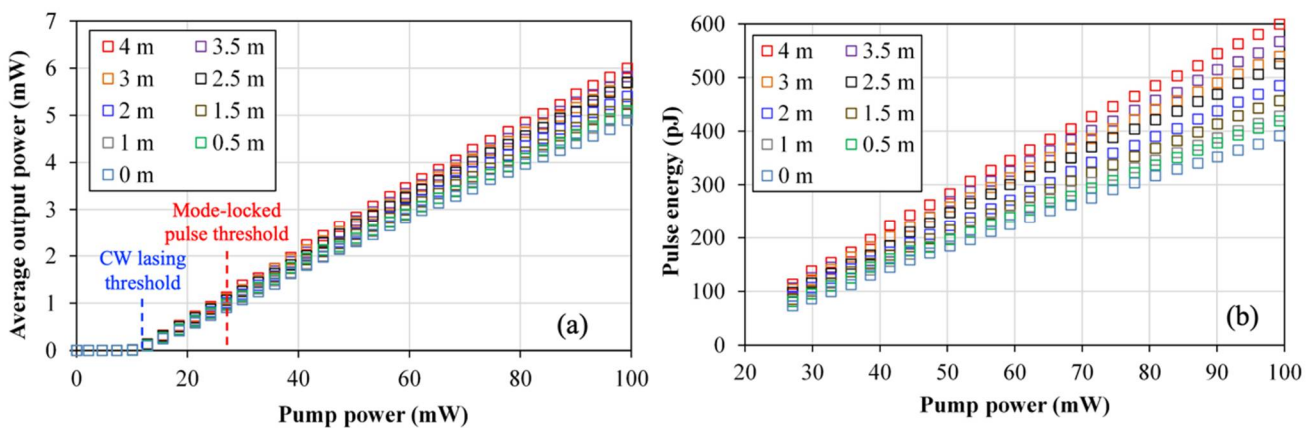


Figure 12. (a) Output power and (b) pulse energy evolution against pump power for different additional SMF-28 lengths.

Table 2. Summary of power development and pulse energy evolution of the mode-locked EDFL at different SMF-28 lengths.

Additional SMF Length (m)	Maximum Average Output Power (mW)	Maximum Pulse Energy (pJ)	Average Output Power Slope Efficiencies (%)
0.0	4.93	391.47	5.70
0.5	5.12	419.25	5.75
1.0	5.01	428.33	5.67
1.5	5.13	456.82	5.80
2.0	5.40	484.93	6.12
2.5	5.26	526.15	5.93
3.0	5.82	539.49	6.41
3.5	5.68	567.28	6.56
4.0	5.99	599.52	6.76

8. Conclusions

We have investigated the dispersion management in graphene/PMMA-based soliton mode-locked fiber lasers within anomalous net cavity dispersion ranging from -0.033 to -0.121 ps² by controlling the length of SMF-28 in the cavity. Experimental outcomes show that shorter SMF-28 length possesses a net cavity GVD value closer to zero. The proposed system is capable of delivering pulse duration from 710 to 820 fs and maximum pulse energy from 391.47 to 599.52 pJ with the increment of SMF-28 length. On the other hand, the spectral bandwidth becomes wider from 5.6 to 8.2 nm with the decrement of SMF-28 length. In addition, the TBP value can be adjusted to be closer to 0.315 by employing a laser cavity with a higher anomalous effect of GVD. This, in turn, can be enhanced by introducing a longer SMF-28 length to give a stronger soliton effect, but with a drawback of longer pulse duration and lower pulse repetition rate generated. In addition, higher average output power and pulse energy are obtained with longer cavity lengths. In terms of pulse stability, as evaluated from the PER measurement, an irregular pattern of PER value is observed against the length of SMF, whereby the optimum PER value is achieved by using 2 m additional SMF length. From this work, it can be concluded that controlling dispersion behavior is an enabling method to optimize the laser operation that suits certain applications, such as frequency metrology, microscopy, and micromachining.

Author Contributions: Conceptualization, A.F.A., K.Y.L. and M.A.M.; methodology, A.F.A., K.Y.L., M.T.A. and M.A.M.; software, K.Y.L.; validation, A.F.A., K.Y.L. and M.A.M.; formal analysis, A.F.A., K.Y.L., W.M.A., M.T.A., F.D.M. and M.A.M.; investigation, A.F.A., K.Y.L., W.M.A., M.T.A., F.D.M. and M.A.M.; resources, A.F.A., M.T.A. and M.A.M.; data curation, K.Y.L.; writing—original draft preparation, K.Y.L. and W.M.A.; writing—review and editing, A.F.A., K.Y.L., W.M.A., M.T.A., F.D.M. and M.A.M.; visualization, A.F.A., K.Y.L., M.T.A. and M.A.M.; supervision, A.F.A., M.T.A. and M.A.M.; project administration, A.F.A., M.T.A. and M.A.M.; funding acquisition, A.F.A. and M.T.A. All authors have read and agreed to the published version of the manuscript.

Funding: National Plan for Science, Technology and Innovation (MAARIFAH), King Abdulaziz City for Science and Technology, Kingdom of Saudi Arabia, Award Number 3-17-09-001-0007.

Institutional Review Board Statement: Not applicable.

Informed Consent Statement: Not applicable.

Data Availability Statement: Not applicable.

Acknowledgments: This project was funded by the National Plan for Science, Technology and Innovation (MAARIFAH), King Abdulaziz City for Science and Technology, Kingdom of Saudi Arabia, Award Number 3-17-09-001-0007.

Conflicts of Interest: The authors declare no conflict of interest.

References

1. Malfondet, A.; Parriaux, A.; Krupa, K.; Millot, G.; Dinda, P.T. Optimum design of NOLM-driven mode-locked fiber lasers. *Opt. Lett.* **2021**, *46*, 1289–1292. [[CrossRef](#)] [[PubMed](#)]
2. Yao, H.; Jing, Z.; Haiying, J.; Mengru, S.; Tianshu, W. Mode-locked fiber laser with multimode fiber as saturable absorber. *Opto-Electron. Eng.* **2021**, *48*, 200362.
3. Ahmad, H.; Ramli, R.; Ismail, N.N.; Aidit, S.N.; Yusoff, N.; Samion, M.Z. Passively mode locked thulium and thulium/holmium doped fiber lasers using MXene Nb₂C coated microfiber. *Sci. Rep.* **2021**, *11*, 1–12. [[CrossRef](#)] [[PubMed](#)]
4. Lau, K.Y.; Hou, D. Recent research and advances of material-based saturable absorber in mode-locked fiber laser. *Opt. Laser Technol.* **2021**, *137*, 106826. [[CrossRef](#)]
5. Guo, B.; Wang, S.-H.; Wu, Z.-X.; Wang, Z.-X.; Wang, D.-H.; Huang, H.; Zhang, F.; Ge, Y.-Q.; Zhang, H. Sub-200 fs soliton mode-locked fiber laser based on bismuthene saturable absorber. *Opt. Express* **2018**, *26*, 22750–22760. [[CrossRef](#)]
6. Debnath, P.; Yeom, D.-I. Ultrafast Fiber Lasers with Low-Dimensional Saturable Absorbers: Status and Prospects. *Sensors* **2021**, *21*, 3676. [[CrossRef](#)]
7. Sun, G.; Feng, M.; Zhang, K.; Wang, T.; Li, Y.; Han, D.; Li, Y.; Song, F. Q-Switched and Mode-Locked Er-doped fiber laser based on MAX phase Ti₂AlC saturable absorber. *Results Phys.* **2021**, *26*, 104451. [[CrossRef](#)]
8. Camarillo-Avilés, A.; López-Estopier, R.; Pottiez, O.; Durán-Sánchez, M.; Ibarra-Escamilla, B.; Jiménez, M.B. Supercontinuum source directly from noise-like pulse emission in a Tm-doped all-fiber laser with nonlinear polarization rotation. *Results Opt.* **2021**, *2*, 100040. [[CrossRef](#)]
9. Liu, G.; Ou, S.; Zhang, Q.; Zhang, M.; Li, X.; Bao, Q. All-polarization-maintaining linear fiber laser mode-locked by nonlinear polarization evolution with phase bias. *Opt. Laser Technol.* **2021**, *142*, 107160. [[CrossRef](#)]
10. Łaszczych, Z.; Soboń, G. Dispersion management of a nonlinear amplifying loop mirror-based erbi-um-doped fiber laser. *Opt. Express* **2021**, *29*, 2690–2702. [[CrossRef](#)]
11. Edelmann, M.; Hua, Y.; Şafak, K.; Kärtner, F.X. Intrinsic amplitude-noise suppression in fiber lasers mode-locked with nonlinear amplifying loop mirrors. *Opt. Lett.* **2021**, *46*, 1752–1755. [[CrossRef](#)] [[PubMed](#)]
12. Gong, Q.; Zhang, H.; Deng, D.; Zu, J. Dissipative Soliton Resonance in an All-Polarization Maintaining Fiber Laser With a Nonlinear Amplifying Loop Mirror. *IEEE Photon. J.* **2020**, *12*, 1–8. [[CrossRef](#)]
13. Yang, Z.; Lustig, E.; Harari, G.; Plotnik, Y.; Lumer, Y.; Bandres, M.A.; Segev, M. Mode-Locked Topological Insulator Laser Utilizing Synthetic Dimensions. *Phys. Rev.* **2020**, *10*, 011059. [[CrossRef](#)]
14. Haris, H.; Arof, H.; Muhammad, A.; Anyi, C.; Tan, S.; Kasim, N.; Harun, S. Passively Q-switched and mode-locked Erbium-doped fiber laser with topological insulator Bismuth Selenide (Bi₂Se₃) as saturable absorber at C-band region. *Opt. Fiber Technol.* **2018**, *48*, 117–122. [[CrossRef](#)]
15. Lee, J.; Lee, J.H. Femtosecond Tm–Ho co-doped fiber laser using a bulk-structured Bi₂Se₃ topological insulator. *Chin. Phys. B* **2018**, *27*, 94219. [[CrossRef](#)]
16. Li, L.; Pang, L.; Wang, Y.; Liu, W. W_xNb_(1-x)Se₂ nanosheets for ultrafast photonics. *Nanoscale* **2021**, *13*, 2511–2518. [[CrossRef](#)]
17. Li, L.; Pang, L.; Zhao, Q.; Wang, Y.; Liu, W. Niobium disulfide as a new saturable absorber for an ultrafast fiber laser. *Nanoscale* **2020**, *12*, 4537–4543. [[CrossRef](#)]
18. Tiu, Z.C.; Ooi, S.I.; Guo, J.; Zhang, H.; Ahmad, H. Application of transition metal dichalcogenide in pulsed fiber laser system. *Mater. Res. Express.* **2019**, *6*, 082004. [[CrossRef](#)]
19. Lee, J.; Lee, K.; Kwon, S.; Shin, B.; Lee, H.J. Investigation of nonlinear optical properties of rhenium diselenide and its application as a femtosecond mode-locker. *Photon. Res.* **2019**, *7*, 984–993. [[CrossRef](#)]
20. Cheng, P.; Du, Y.; Han, M.; Shu, X. Mode-locked and Q-switched mode-locked fiber laser based on a ferroferric-oxide nanoparticles saturable absorber. *Opt. Express* **2020**, *28*, 13177–13186. [[CrossRef](#)]
21. Wang, W.; Yue, W.; Liu, Z.; Shi, T.; Du, J.; Leng, Y.; Wei, R.; Ye, Y.; Liu, C.; Liu, X.; et al. Ultrafast Nonlinear Optical Response in Plasmonic 2D Molybdenum Oxide Nanosheets for Mode-Locked Pulse Generation. *Adv. Opt. Mater.* **2018**, *6*, 1–8. [[CrossRef](#)]
22. Fu, B.; Sun, J.; Wang, C.; Shang, C.; Xu, L.; Li, J.; Zhang, H. MXenes: Synthesis, Optical Properties, and Applications in Ultrafast Photonics. *Small* **2021**, *17*, 2006054. [[CrossRef](#)] [[PubMed](#)]
23. Guo, B.; Xiao, Q.; Wang, S.; Zhang, H. 2D Layered Materials: Synthesis, Nonlinear Optical Properties, and Device Applications. *Laser Photon. Rev.* **2019**, *13*, 1800327. [[CrossRef](#)]
24. Fu, B.; Sun, J.; Wang, G.; Shang, C.; Ma, Y.; Ma, J.; Xu, L.; Scardaci, V. Solution-processed two-dimensional materials for ultrafast fiber lasers (invited). *Nanophotonics* **2020**, *9*, 2169–2189. [[CrossRef](#)]
25. Ma, C.; Wang, C.; Gao, B.; Adams, J.; Wu, G.; Zhang, H. Recent progress in ultrafast lasers based on 2D materials as a saturable absorber. *Appl. Phys. Rev.* **2019**, *6*, 041304. [[CrossRef](#)]
26. Bao, Q.; Zhang, H.; Wang, Y.; Ni, Z.; Yan, Y.; Shen, Z.X.; Loh, K.P.; Tang, D.Y. Atomic-Layer Graphene as a Saturable Absorber for Ultrafast Pulsed Lasers. *Adv. Funct. Mater.* **2009**, *19*, 3077–3083. [[CrossRef](#)]
27. Sun, Z.; Hasan, T.; Torrisi, F.; Popa, D.; Privitera, G.; Wang, F.; Bonaccorso, F.; Basko, D.M.; Ferrari, A.C. Graphene Mode-Locked Ultrafast Laser. *ACS Nano* **2010**, *4*, 803–810. [[CrossRef](#)]
28. Ponarina, M.; Okhrimchuk, A.; Alagashev, G.; Orlova, G.; Dolmatov, T.; Rybin, M.; Obratsova, E.; Bukin, V.; Obratsov, P. Wavelength-switchable 9.5 GHz graphene mode-locked waveguide laser. *Appl. Phys. Express* **2021**, *14*, 072001. [[CrossRef](#)]

29. Hua, K.; Wang, D.N. Coupling scheme for graphene saturable absorber in a linear cavity mode-locked fiber laser. *Opt. Lett.* **2021**, *46*, 4362–4365. [[CrossRef](#)]
30. Peng, X.; Yan, Y. Graphene saturable absorbers applications in fiber lasers. *J. Eur. Opt. Soc. Publ.* **2021**, *17*, 1–26. [[CrossRef](#)]
31. Terra, O.; Hussein, H.M.; Kotb, H. Soliton mode-locked fiber laser for distance measurements. *Appl. Opt.* **2021**, *60*, 3452–3457. [[CrossRef](#)] [[PubMed](#)]
32. de Faria, A.C.A. Optical Sensor for Nonlinear and Quantum Optical Effects. In *Nonlinear Optics—From Solitons to Similaritons*; IntechOpen: London, UK, 2021; Available online: <https://www.intechopen.com/chapters/70829> (accessed on 3 January 2022). [[CrossRef](#)]
33. Voloshin, A.S.; Kondratiev, N.M.; Lihachev, G.V.; Liu, J.; Lobanov, V.E.; Dmitriev, N.Y.; Weng, W.; Kippenberg, T.J.; Bilenko, I.A. Dynamics of soliton self-injection locking in optical microresonators. *Nat. Commun.* **2021**, *12*, 1–10. [[CrossRef](#)] [[PubMed](#)]
34. Lin, Y.-S.; Wang, C.-C.; Chen, C.-C.; Hsiao, C.-C.; Chou, Y.-H. A high-performance ibc-Hub transceiver for intra-body communication system. *Microw. Opt. Technol. Lett.* **2012**, *54*, 1143–1153. [[CrossRef](#)]
35. Luo, H.; Yang, J.; Li, J.; Liu, Y. Tunable sub-300 fs soliton and switchable dual-wavelength pulse generation from a mode-locked fiber oscillator around 28 μm . *Opt. Lett.* **2021**, *46*, 841–844. [[CrossRef](#)] [[PubMed](#)]
36. Dai, R.; Meng, Y.; Li, Y.; Qin, J.; Zhu, S.; Wang, F. Nanotube mode-locked, wavelength and pulsewidth tunable thulium fiber laser. *Opt. Express* **2019**, *27*, 3518–3527. [[CrossRef](#)]
37. Zhu, J.; Ge, S.; Wang, J.; Zhang, W.; Ren, H.; Yan, B. Systematic exploration and characterization on the influence of dispersion to pulse characteristics in Tm-doped NPE mode-locked fiber oscillator. *Infrared Phys. Technol.* **2021**, *115*, 103722. [[CrossRef](#)]
38. Pawliszewska, M.; Martynkien, T.; Przewłoka, A.; Sotor, J. Dispersion-managed Ho-doped fiber laser mode-locked with a graphene saturable absorber. *Opt. Lett.* **2019**, *7*, 36–41. [[CrossRef](#)]
39. Fu, B.; Hua, Y.; Xiao, X.; Zhu, H.; Sun, Z.; Yang, C. Broadband Graphene Saturable Absorber for Pulsed Fiber Lasers at 1, 1.5, and 2 μm . *IEEE J. Sel. Top. Quantum Electron.* **2014**, *20*, 411–415. [[CrossRef](#)]
40. Garmire, E. Resonant optical nonlinearities in semiconductors. *IEEE J. Sel. Top. Quantum Electron.* **2000**, *6*, 1094–1110. [[CrossRef](#)]
41. Sun, Z.; Hasan, T.; Wang, F.; Rozhin, A.G.; White, I.H.; Ferrari, A.C. Ultrafast stretched-pulse fiber laser mode-locked by carbon nanotubes. *Nano Res.* **2010**, *3*, 404–411. [[CrossRef](#)]
42. Wright, M.W.; Yao, H.; Marciante, J.R. Resonant pumping of Er-doped fiber amplifiers for improved laser efficiency in free-space optical communications. *NASA IPN Prog. Rep.* **2012**, *11*, 42–189.
43. Sotor, J.; Pasternak, I.; Krajewska, A.; Strupinski, W.; Sobon, G. Sub-90 fs a stretched-pulse mode-locked fiber laser based on a graphene saturable absorber. *Opt. Express* **2015**, *23*, 27503–27508. [[CrossRef](#)] [[PubMed](#)]
44. Tarka, J.; Boguslawski, J.; Sobon, G.; Pasternak, I.; Sotor, J.; Przewłoka, A.; Strupinski, W.; Abramski, K.M. Power Scaling of an All-PM Fiber Er-Doped Mode-Locked Laser Based on Graphene Saturable Absorber. *IEEE J. Sel. Top. Quantum Electron.* **2016**, *23*, 60–65. [[CrossRef](#)]
45. Chen, H.R.; Tsai, C.-Y.; Chang, C.-Y.; Lin, K.-H.; Chang, C.-S.; Hsieh, W.-F. Investigation of Graphene Dispersion from Kelly Sideband in Stable Mode-Locked Erbium-Doped Fiber Laser by Few-Layer Graphene Saturable Absorbers. *J. Light. Technol.* **2015**, *33*, 4406–4412. [[CrossRef](#)]